

FDTD Investigation on Electromagnetic Scattering from Two-Dimensional Layered Rough Surfaces

Juan Li, Li Xin Guo, and Hao Zeng

School of Science
Xidian University, No. 2, Taibai Road, Xi'an, Shaanxi, China

lijuan029@yeah.net, lxguo@mail.xidian.edu.cn, tsanghao@foxmail.com

Abstract— This paper presents an investigation into the electromagnetic scattering characteristic of two-dimensional (2-D) layered rough surfaces by using a finite-difference time-domain (FDTD) algorithm, which constitutes a three-dimensional scattering problem. The uniaxial perfectly matched layer medium is adopted for truncation of FDTD lattices, in which the finite-difference equations can be used for the total computation domain by properly choosing the uniaxial parameters. The upper and down rough surfaces are characterized with Gaussian statistics for the height and the autocorrelation function. The angular distribution of bistatic scattering coefficient from a 2-D single-layered rough surface is calculated, and it shows good agreement with the numerical result through the Kirchhoff Approximation except for with large scattering angles. Finally, the bistatic scattering coefficients versus scattered and azimuthal angle for different conditions are analyzed in detail.

Index Terms— Finite difference time domain (FDTD), electromagnetic scattering, rough surface.

I. INTRODUCTION

The electromagnetic scattering from a randomly rough surface has attracted considerable interest in the fields of radar surveillance, surface physics, and remote sensing of the ocean and soil. The analytical technique [1] and numerical techniques [2-3] have been developed for the efficient analysis of scattering by a single-layered rough surface. However, when the electromagnetic wave is incident on stratified soil, sand cover of arid regions, or ice and oil on the sea surface, it is necessary to investigate the scattering from multilayered rough surfaces. There have been some studies on the scattering from layered rough surfaces in recent years. Tabatabaenejad, et al. [4]

analyzed the bistatic scattering from two-dimensional (2-D) stratified rough surfaces by using the small perturbation method (SPM). Some numerical methods are also used to solve the scattering characteristic from 1-D or 2-D layered medium, such as the forward-backward method with spectral acceleration [5], the extended boundary condition method (EBCM) [6], and the steepest descent fast multipole method (SDFMM) [7]. In this paper, the finite-difference time-domain (FDTD) algorithm is utilized to analyze the electromagnetic scattering from 2-D layered rough surfaces. As for the FDTD algorithm applying to rough surface scattering is concerned, Hastings *et al.* analyzed the scattering from 1-D rough surface using the FDTD method with PML absorbing boundary [8]. Kuang et al. adopted the FDTD method to study the composite scattering from a target above the 2-D periodic rough surface [9]. In our previous work, this method with Mur and UPML absorbing boundary was utilized to solve the composite scattering from a target above 1-D randomly rough surface [10, 11]. Comparing the FDTD algorithm with other numerical methods, there are some advantages: the rough surface may be PEC and dielectric, which is due to the reason that any other change need not be done in the original FDTD code except the part where the material constants are set in each cell. In addition, the results obtained by this method are in the time domain, and can indicate both the transient behavior as well as the steady state.

In the paper, the uniaxial perfectly matched layer (UPML) medium is adopted for truncation of FDTD lattices. In the uniaxial medium the finite-difference equations are suitable for the whole computation domain due to the field satisfy Maxwell's equations, which makes the problem simple. The paper is organized as follows: the theoretical formulae of calculating scattering fields

by FDTD are developed in Section II. The bistatic scattering coefficient versus scattered and azimuthal angle are presented and discussed in Section III for different conditions. Section IV ends with the conclusions of the paper and proposes further investigations in this topic.

II. BISTATIC SCATTERING FROM 2-D LAYERED ROUGH SURFACES

The geometry for 2-D layered rough surfaces is shown in Fig. 1, where the scattering model is composed of three homogeneous layers: the air, the upper medium layer with the finite thickness H , and the lower medium layer with infinite depth. The upper interface $f_1(x, y)$ and lower interface $f_2(x, y)$ are characterized with Gaussian statistics for the height and the autocorrelation function. The parameters ϵ_1 , ϵ_2 represent the relative dielectric constants of the upper medium layer and the lower medium layer, respectively.

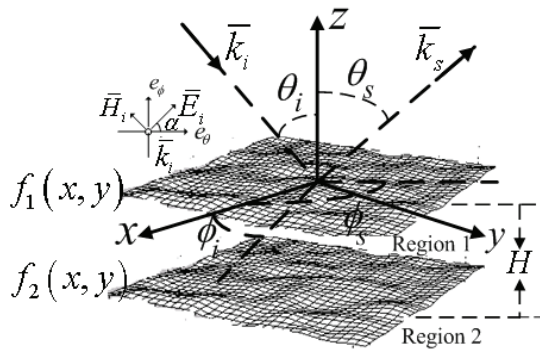


Fig. 1. Geometry of 2-D layered rough surfaces.

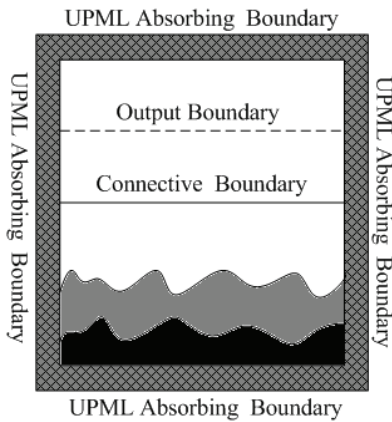


Fig. 2. Division model of computation region for the FDTD algorithm.

A. Simulation of Rough Surface and FDTD

Model

In this section, a two-dimensional Gaussian randomly rough interface is simulated by Monte Carlo method [12]. It is assumed that the size of the rough surface is $S = L \times L$, and N is the number of the points discretized in the x - and y -directions. The rough surface profile $f(x, y)$ is expressed as:

$$f(x, y) = \frac{1}{L \times L} \sum_{m=-\frac{N}{2}}^{\frac{N}{2}-1} \sum_{n=-\frac{N}{2}}^{\frac{N}{2}-1} F(K_{xm}, K_{yn}) \exp(iK_{xm}x + iK_{yn}y) \quad (1)$$

$$F(K_{xm}, K_{yn}) = 2\pi L \sqrt{W(K_{xm}, K_{yn})} \begin{cases} \frac{N(0,1) + j_0 N(0,1)}{\sqrt{2}}, & m, n \neq 0, \frac{N}{2} \\ N(0,1) & m \text{ or } n = 0, \frac{N}{2} \end{cases} \quad (2)$$

where $j_0 = \sqrt{-1}$, $K_{xm} = \frac{2\pi m}{L}$ and $K_{yn} = \frac{2\pi n}{L}$ are the discrete set of spatial frequencies. To generate a real sequence, the requirement for $F(K_{xm}, K_{yn})$ is as follows

$$F(K_{xm}, K_{yn}) = F^*(-K_{xm}, -K_{yn}) \quad (3a)$$

$$F(K_{xm}, -K_{yn}) = F^*(-K_{xm}, K_{yn}) \quad (3b)$$

$W(K_{xm}, K_{yn})$ is the power spectral density function of Gaussian rough surface [12] given by:

$$W(K_{xm}, K_{yn}) = \frac{l_x l_y h^2}{4\pi} \exp\left(-\frac{K_{xm}^2 l_x^2}{4} - \frac{K_{yn}^2 l_y^2}{4}\right), \quad (4)$$

where, h is the root mean square (rms) of random surface height. l_x and l_y are the correlation lengths along the x - and y -directions.

It is important for us to know the division of the computation region with FDTD algorithm in calculating electromagnetic scattering from 2-D layered rough surfaces. Figure 2 shows the section plane along the x direction of the FDTD computation region. The incident wave is generated on the connective boundary, and the UPML absorbing medium is the outer boundary of FDTD region. In addition, the output boundary must be set to do a near-to-far transformation to obtain the far fields.

B. UPML Absorbing Boundary

In theory, the computational domain should be unbounded due to the scattered field existing in the infinite free space, but no computer can store an unlimited amount of data. To deal with the conflict, a virtual absorbing boundary must be built, and the outgoing waves have to propagate outward without non-physical reflection from the boundary. There have been many absorbing boundary conditions developed to implement this in the FDTD algorithm. Where, the UPML absorbing medium [13] is used to terminate the FDTD lattices, in which the finite-difference equations can be used for the total computation domain due to the fields satisfying Maxwell's equations (Ampere's law and Faraday's law). This makes the algorithm efficient since one does not have to take special care of the interface plane between the boundary and the interior regions. In addition, the uniaxial medium can be perfectly matched to an interior lossy medium without any modification except for properly choosing the uniaxial parameters. In the uniaxial medium, Ampere's law and Faraday's law in the xyz coordinate are expressed as

$$\begin{cases} \frac{\partial H_z}{\partial y} - \frac{\partial H_y}{\partial z} = (j_0 w \varepsilon_1 + \sigma_1) \frac{s_y s_z}{s_x} E_x \\ \frac{\partial H_x}{\partial z} - \frac{\partial H_z}{\partial x} = (j_0 w \varepsilon_1 + \sigma_1) \frac{s_x s_z}{s_y} E_y \\ \frac{\partial H_y}{\partial x} - \frac{\partial H_x}{\partial y} = (j_0 w \varepsilon_1 + \sigma_1) \frac{s_x s_y}{s_z} E_z \end{cases} \quad (5a)$$

$$\begin{cases} \frac{\partial E_z}{\partial y} - \frac{\partial E_y}{\partial z} = -j_0 w \mu_1 \frac{s_y s_z}{s_x} H_x \\ \frac{\partial E_x}{\partial z} - \frac{\partial E_z}{\partial x} = -j_0 w \mu_1 \frac{s_x s_z}{s_y} H_y \\ \frac{\partial E_y}{\partial x} - \frac{\partial E_x}{\partial y} = -j_0 w \mu_1 \frac{s_x s_y}{s_z} H_z \end{cases} \quad (5b)$$

where, ε_1 , μ_1 , σ_1 represent the electrical permittivity, the magnetic permeability, and the electric conductivity in the interior medium. s_x , s_y and s_z are only spatially variant along the x , y , and z directions, $s_x = k_x + \sigma_x / j_0 w \varepsilon_0$, $s_y = k_y + \sigma_y / j_0 w \varepsilon_0$, and $s_z = k_z + \sigma_z / j_0 w \varepsilon_0$, referring to [13]. In equation(5), for Ampere's law the intermediate variables P'_x, P'_y, P'_z and P_x, P_y, P_z

are introduced as

$$P'_x = \frac{s_y s_z}{s_x} E_x, \quad P'_y = \frac{s_x s_z}{s_y} E_y, \quad P'_z = \frac{s_y s_x}{s_z} E_z \quad (6)$$

$$P_x = P'_x / s_y, \quad P_y = P'_y / s_z, \quad P_z = P'_z / s_x \quad (7)$$

and for Faraday's law, the intermediate variables B_x, B_y , and B_z are inserted

$$B_x = \mu_1 \frac{s_z}{s_x} H_x, \quad B_y = \mu_1 \frac{s_x}{s_y} H_y, \quad B_z = \mu_1 \frac{s_y}{s_z} H_z. \quad (8)$$

Using a Fourier transform where $j_0 w \rightarrow \partial / \partial t$, the equations above can be transformed into the time domain. Thus, in Ampere's law the electric fields in the constant x plane are obtained by the following relations $H_y, H_z \rightarrow P'_x \rightarrow P_x \rightarrow E_x$, i.e.,

$$\frac{\partial H_z}{\partial y} - \frac{\partial H_y}{\partial z} = \varepsilon_1 \frac{\partial P'_x}{\partial t} + \sigma_1 P'_x \quad (9a)$$

$$\frac{\partial P'_x}{\partial t} = k_y \frac{\partial P_x}{\partial t} + \frac{\sigma_y}{\varepsilon_0} P_x \quad (9b)$$

$$k_x \frac{\partial P_x}{\partial t} + \frac{\sigma_x}{\varepsilon_0} P_x = k_z \frac{\partial E_x}{\partial t} + \frac{\sigma_z}{\varepsilon_0} E_x. \quad (9c)$$

Similarly, in Faraday's law the magnetic field in the constant x plane is deduced by the relations $E_y, E_z \rightarrow B_x \rightarrow H_x$

$$\frac{\partial E_z}{\partial y} - \frac{\partial E_y}{\partial z} = -k_y \frac{\partial B_x}{\partial t} - \frac{\sigma_y}{\varepsilon_0} B_x \quad (10a)$$

$$k_x \frac{\partial B_x}{\partial t} + \frac{\sigma_x}{\varepsilon_0} B_x = \mu_1 k_z \frac{\partial H_x}{\partial t} + \frac{\mu_1}{\varepsilon_0} \sigma_z H_x. \quad (10b)$$

For planes of constant y or constant z the uniaxial parameters are simply permuted and similar expressions can easily be derived.

C. Connective Boundary

The connective boundary divides the computation region into the total field region and the scattered field region. The total field region contains the incident field and the scattered field, but the scattered field region only includes the scattered field [14]. It will be shown how the incident wave is generated on the connective boundary and limited in total field region.

In Fig. 1, a plane wave $\vec{E}_i = \vec{E}_0 \exp(-j_0 \vec{k}_i \cdot \vec{r} + j_0 w t)$ propagates in the direction of \vec{k}_i . The incidence direction \vec{k}_i makes angles θ_i relative to the z -axis, and ϕ_i relative to the x -axis. The unit vector \hat{E}_0 is the unit polarization direction. The

polarization direction is rotated counter clockwise by the angle α (i.e. the polarization angle) from e_θ within the incidence plane. The incident wave is computed using the 1-D FDTD method [14] with the same spatial step $\Delta x = \Delta y = \Delta z = \delta$ and temporal step Δt as the 3-D FDTD method mentioned above. Where, Δx , Δy , Δz are the spatial increments in the x -, y - and z -directions. To ensure the stability and accuracy of the FDTD algorithm, $\Delta t = 0.5 \times \delta/c$ is presented to satisfy the Courant stability criterion in [15] and c is the light speed propagation in the vacuum.

Let $E_{x,i}^n$, $E_{y,i}^n$, $H_{x,i}^n$ and $H_{y,i}^n$ be the incident electrical and magnetic fields at the connective boundary. The finite-difference equations on the connective boundary should then be updated as:

$$E_x^{n+1}\left(i, j + \frac{1}{2}, k\right) = E_x^n\left(i, j + \frac{1}{2}, k\right) + \frac{\Delta t}{\epsilon} [\nabla \times \bar{H}]_x^{n+1/2} - \frac{\Delta t}{\epsilon} \frac{H_{y,i}^{n+1/2}\left(i + \frac{1}{2}, j, k + \frac{1}{2}\right)}{\Delta z} \quad (11)$$

$$E_y^{n+1}\left(i, j + \frac{1}{2}, k\right) = E_y^n\left(i, j + \frac{1}{2}, k\right) + \frac{\Delta t}{\epsilon} [\nabla \times \bar{H}]_y^{n+1/2} + \frac{\Delta t}{\epsilon} \frac{H_{x,i}^{n+1/2}\left(i, j + \frac{1}{2}, k + \frac{1}{2}\right)}{\Delta z} \quad (12)$$

$$H_x^{n+1/2}\left(i, j + \frac{1}{2}, k + \frac{1}{2}\right) = H_x^{n-1/2}\left(i, j + \frac{1}{2}, k + \frac{1}{2}\right) - \frac{\Delta t}{\epsilon} [\nabla \times \bar{H}]_x^n + \frac{\Delta t}{\mu} \frac{E_{y,i}^n\left(i, j + \frac{1}{2}, k\right)}{\Delta z} \quad (13)$$

$$H_y^{n+1/2}\left(i + \frac{1}{2}, j, k + \frac{1}{2}\right) = H_y^{n-1/2}\left(i + \frac{1}{2}, j, k + \frac{1}{2}\right) - \frac{\Delta t}{\epsilon} [\nabla \times \bar{H}]_y^n - \frac{\Delta t}{\mu} \frac{E_{x,i}^n\left(i + \frac{1}{2}, j, k\right)}{\Delta z} \quad (14)$$

In numerical simulations, a finite-length rough surface must be used to model scattering from the infinite surface. When a plane wave strikes the finite-length rough surface, boundary reflection

occurs. One way of minimizing reflection is to construct an incident wave that tapers to very small values at the surface edges. Reflection still occurs and cannot be completely eliminated, but it makes negligible contributions to the scattered field. To solve this problem, Fung et al. put forward the Gaussian window function [16] to guard against the truncation effect, and the Gaussian window function is written as

$$G(x, y) = \exp\left\{-\left[(x-x_0)^2 + (y-y_0)^2\right] \left(\frac{\cos\theta_i}{T}\right)^2\right\} \quad (15)$$

where x_0 and y_0 are the spatial coordinates at the center of the connective boundary, T is a constant which determines the width of the window function, $\cos\theta_i/T = 2.6/\rho_m$ and ρ_m is the minimum distance from the center (x_0, y_0) to the edge surface.

D. Output Boundary

The near fields for the rough surface can be obtained on the basis of theory described above. As indicated in [14], a way to obtain the far field is to do a near-to-far field transformation, which is based on the surface equivalence theorem. The transform formula for the output boundary is expressed as

$$\bar{E}_\theta = \hat{\theta}(-j_0 k_0 \frac{\exp(-j k_0 r)}{4\pi r}) [z_0 f_x \cos\theta_s \cos\phi_s + z_0 f_y \cos\theta_s \sin\phi_s + (-f_{mx} \sin\phi_s + f_{my} \cos\phi_s)] \quad (16)$$

$$\bar{E}_\phi = \hat{\phi} j_0 k_0 \frac{\exp(-j_0 k_0 r)}{4\pi r} [z_0 f_x \sin\phi_s - z_0 f_y \cos\phi_s + f_{mx} \cos\theta_s \cos\phi_s + f_{my} \cos\theta_s \sin\phi_s] \quad (17)$$

where k_0 is the incident wave number (i.e., $k_0 = |\vec{k}_i|$). r is the distance from the origin of the xyz -coordinate to any point at infinity and z_0 is the wave impedance in free space. ϕ_s represents the scattered azimuthal angle, and θ_s is the scattered angle. The terms f_x , f_y , f_{mx} , and f_{my} are related to equivalent surface electric and magnetic currents [14]. In the paper, we choose the incident plane xoz (see Fig. 1) as the reference plane. Thus, the horizontal polarization wave is incidence on a 2-D rough surface when the incident electric field \bar{E}_i is in the plane xoz (i.e. $\alpha = 0^\circ$). Otherwise, the vertical polarization wave is considered (i.e.

$\alpha = 90^\circ$). The bistatic scattering coefficient [17] in the far zone is shown as

$$\sigma_{HH} = \lim_{r \rightarrow \infty} \frac{4\pi r^2}{S} \frac{|\bar{E}_\theta|^2}{|\bar{E}_i|^2}, \sigma_{VH} = \lim_{r \rightarrow \infty} \frac{4\pi r^2}{S} \frac{|\bar{E}_\phi|^2}{|\bar{E}_i|^2} \quad (\alpha = 0^\circ) \quad (18a)$$

$$\sigma_{HV} = \lim_{r \rightarrow \infty} \frac{4\pi r^2}{S} \frac{|\bar{E}_\theta|^2}{|\bar{E}_i|^2}, \sigma_{VV} = \lim_{r \rightarrow \infty} \frac{4\pi r^2}{S} \frac{|\bar{E}_\phi|^2}{|\bar{E}_i|^2} \quad (\alpha = 90^\circ) \quad (18b)$$

III. NUMERICAL RESULTS AND DISCUSSIONS

In this section, the numerical results of basic scattering from a 2-D two-layered rough surface for different conditions are discussed in detail. For convenience, some parameters describing the rough surface are measured in wave length λ , and $S = 25.6\lambda \times 25.6\lambda$. The spatial increment is taken as $\Delta x = \Delta y = \Delta z = \delta = \lambda/10$. The PML

The randomly rough surface is created by 10 Monte Carlo realizations and it is assumed that the horizontal incident wave is considered (i.e., $\alpha = 0^\circ$). The incident azimuthal angle is $\phi_i = 180^\circ$, and incident frequency is 0.3GHz in the following results.

In order to ensure the validity of FDTD algorithm presented in the paper, in Fig. 3 we first compute the angular distribution of bistatic scattering coefficient from 2-D PEC and dielectric single-layered rough surface using the Kirchhoff Approximation (KA) and FDTD, respectively. The incident angle is 20° and the bistatic HH polarized scattering is considered. The rms height and correlation length of rough surface is given by $h = 0.1\lambda$ and $l_x = l_y = 1.0\lambda$. The relative dielectric constant of dielectric rough surface is $\epsilon_r = (2.5, 0.18)$. The results from KA are obtained by introducing the 2-D tapered incident wave [18] instead of the plane wave into the classical Kirchhoff approximation [19].

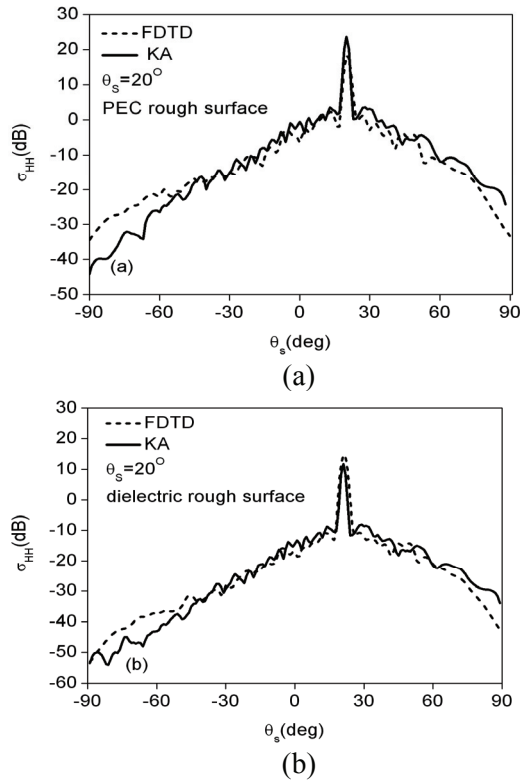


Fig. 3. Comparison of the two different methods for the bistatic scattering from 2-D single-layered rough surface, $\theta_i = 20^\circ$ (a) PEC (b) dielectric. thickness is 5δ .

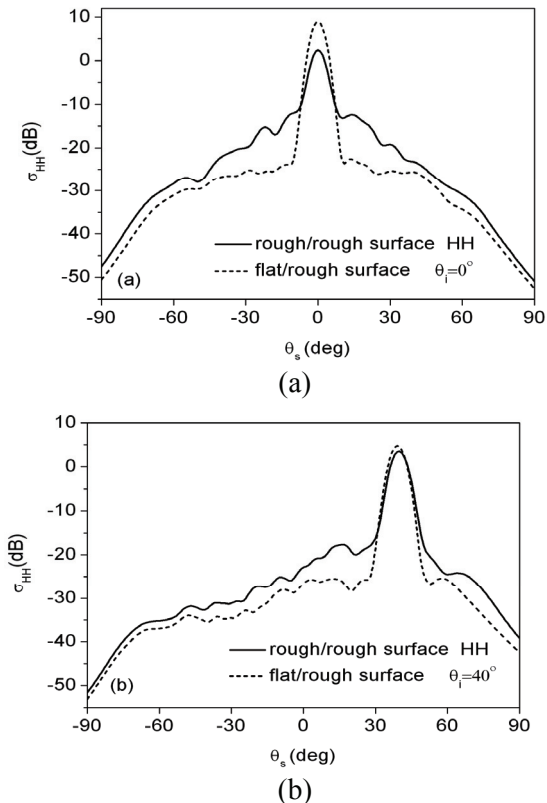


Fig. 4. The angular distribution of bistatic scattering coefficient for the different roughness of upper interface (a) $\theta_i = 0^\circ$, (b) $\theta_i = 40^\circ$.

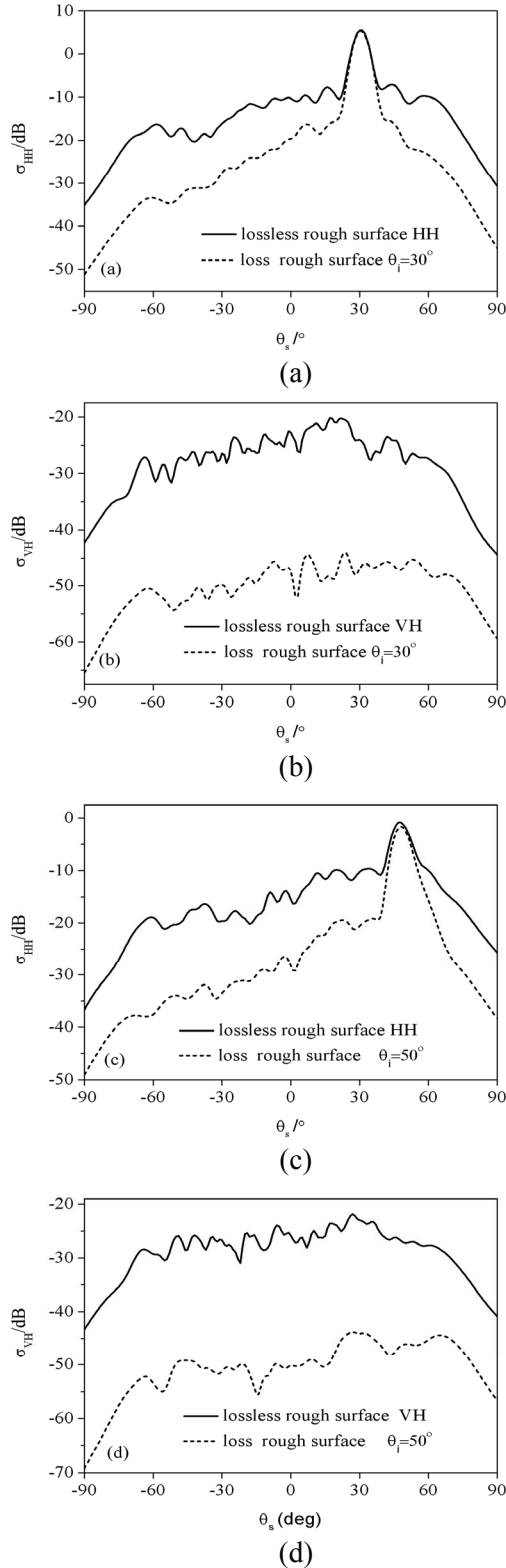


Fig. 5. Bistatic scattering coefficient from the two-layered lossless/ loss rough surface (a) HH $\theta_i = 30^\circ$ (b) VH $\theta_i = 30^\circ$ (c) HH $\theta_i = 50^\circ$ (d) VH $\theta_i = 50^\circ$.

It is obvious that the angular distribution of scattering coefficient for both the PEC (Fig. 3(a)) and dielectric (Fig. 3(b)) rough surface by FDTD is in good agreement with that obtained by KA except for the large scattering angles, which demonstrates the feasibility and applicability of FDTD algorithm.

Figure 4 presents the angular distribution of bistatic scattering coefficient for the case of the upper interface is flat but the lower interface is rough (i.e., flat/rough, $h_2 = 0.2\lambda$, $l_{2x} = l_{2y} = 1.3\lambda$), and for the case of both the two interfaces are rough (i.e., rough/rough, $h_1 = 0.1\lambda$, $l_{1x} = l_{1y} = 1.0\lambda$, $h_2 = 0.2\lambda$, $l_{2x} = l_{2y} = 1.3\lambda$). The thickness of upper medium layer is $H = 2\lambda$ where the results for HH polarization are given for both the incident angle 0° (Fig. 4 (a)) and 40° (Fig. (b)). The relative dielectric constant of upper medium layer is $\epsilon_1 = (3.7, 0.13)$, and that of the lower medium layer is $\epsilon_2 = (16.16, 1.15)$ [20]. It is shown that the bistatic scattering from a rough/rough surface is stronger than that of a flat/rough surface for all the scattering angles except for the specular direction. In the large scattered direction, the latter is relatively approach to the former.

In Fig. 5, co-polarized (HH) and cross-polarized (VH) bistatic scattering coefficients from two-layered lossless/loss rough surfaces ($h_1 = 0.1\lambda$, $l_{1x} = l_{1y} = 1.0\lambda$, $h_2 = 0.2\lambda$, $l_{2x} = l_{2y} = 1.3\lambda$, $H = 2\lambda$) are investigated for the different incident angles, where the dielectric constant of lossless rough surfaces is $\epsilon_1 = 3.7$, $\epsilon_2 = 16.16$, and that of lossy rough surfaces is $\epsilon_1 = (3.7, 0.13)$, $\epsilon_2 = (16.16, 1.15)$. As the HH polarization (Fig. 5(a) and Fig. 5(c)) is concerned, it is easily observed that the bistatic scattering coefficient from two-layered lossless rough surfaces is much greater than the result of two-layered lossy rough surfaces for the scattered angles except for the specular direction. But for VH polarization (Fig. 5 (b) and Fig. 5 (d)), the scattering from lossless layered rough surfaces is larger than that of lossy rough surfaces over the whole scattered angles range.

To further explore the important scattering characteristics of 2-D layered rough surfaces, the azimuthal variation of bistatic HH- and VH-polarized scattering coefficients are investigated for different scattered angles in Fig. 6. The

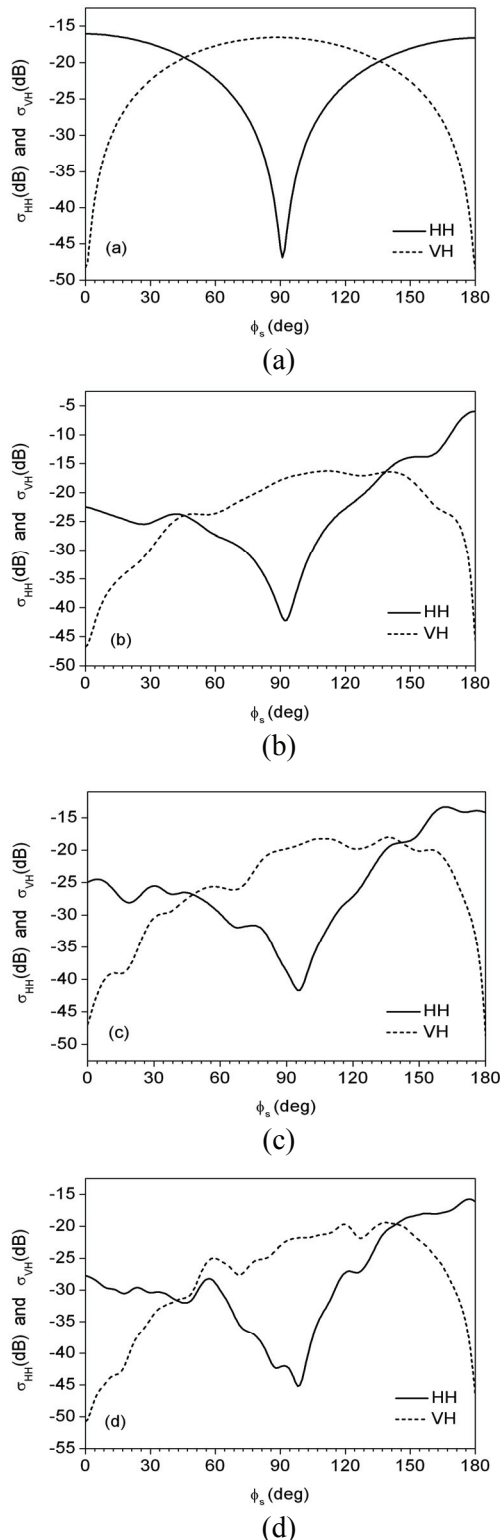


Fig. 6. The azimuthal distribution of bistatic scattering coefficient from two-layered rough surfaces $\theta_i = 20^\circ$ (a) $\theta_s = 5^\circ$ (b) $\theta_s = 15^\circ$ (c) $\theta_s = 30^\circ$ (d) $\theta_s = 45^\circ$.

parameters of rough surface are identical to the data in Fig. 5. The incident angle 20° is considered. It is shown that the angular distribution from HH-polarized scattering coefficients reaches a maximum in the neighborhood where the VH polarization is a minimum and vice versa in Fig.6. In addition, it is observed that the azimuthal angular pattern of the scattered angle 0° is nearly symmetric for both HH polarization and VH polarization, but the minimum of HH polarization and the maximum of VH polarization begin to shift towards the forward direction ($\phi_s = 180^\circ$) for the other scattering angles.

IV. CONCLUSIONS

This paper presents a study of electromagnetic scattering from 2-D layered rough surfaces by using FDTD algorithm. At first, the basic theory of FDTD method for calculating the scattered field is developed, including the generation of incident wave, the UPML absorbing boundary conditions, and a transform from near- to far- field on the output boundary. Then the numerical results of bistatic scattering coefficient versus scattered and azimuthal angle for different conditions are shown and analyzed in detail. Future investigation will include the electromagnetic scattering from 2-D layered rough surfaces with a large-scale rough surface and a large incident angle.

ACKNOWLEDGEMENT

This work was supported by the National Natural Science Foundation of China (Grant No. 60571058) and the Specialized Research Fund for the Doctoral Program of Higher Education, China (20070701010).

REFERENCES

- [1] T. M. Elfouhaily and J. T. Johnson, "A New Model for Rough Surface Scattering," *IEEE Trans. Geosci. Remote Sensing*, vol. 45, no. 7, pp. 2300-2308, 2007.
- [2] R. L. Wagner, J. M. Song, and W. C. Chew, "Monte Carlo Simulation of Electromagnetic Scattering from Two-Dimensional Random Rough Surfaces," *IEEE Trans. Antennas Propag.*, vol. 45, no. 2, pp. 235-245, 1997.
- [3] S. Q. Li, C. H. Chan, M. Y. Xia, B. Zhang, and L. T. Sang, "Multilevel expansion of the

- sparse-matrix canonical grid method for two-dimensional random rough surfaces,” *IEEE Trans. Antennas Propag.*, vol. 49, no. 11, pp. 1579-1589, 2001.
- [4] A. Tabatabaenejad and M. Moghaddam, “Bistatic scattering from three-dimensional layered rough surfaces,” *IEEE Trans. Geosci. Remote Sensing*, vol. 44, no. 8, pp. 2102-2114, 2006.
- [5] C. D. Moss, T. M. Grzegorzczak, H. C. Han, and J. A. Kong, “Forward-backward method with spectral acceleration for scattering from layered rough surfaces,” *IEEE Trans. Antennas Propag.*, vol. 54, no. 3, pp. 1006-1016, 2006.
- [6] C. H. Kuo and M. Moghaddam, “Scattering from multilayer rough surfaces based on the extended boundary condition method and truncated singular value decomposition,” *IEEE Trans. Antennas Propag.*, vol. 54, no. 10, pp.2917-2929, 2006.
- [7] M. E. Shenawee, “Polarimetric scattering from two-layered two-dimensional random rough surfaces with and without buried objects,” *IEEE Trans. Geosci. Remote Sensing*, vol. 52, no. 1, pp. 67-76, 2005.
- [8] F. D. Hastings, J. B. Schneider, and S. L. Broschat, “A Monte-Carlo FDTD technique for rough surface scattering,” *IEEE Trans. Antennas Propag.*, vol. 43, no. 11, pp. 1183-1191, 1995.
- [9] L. Kuang and Y. Q. Jin, “Bistatic scattering from a three-dimensional object over a randomly rough surface using the FDTD algorithm,” *IEEE Trans. Antennas Propag.*, vol. 55, no. 8, pp. 2302-2312, 2007.
- [10] J. Li, L. X. Guo and H. Zeng, “FDTD investigation on the electromagnetic scattering from a target above a randomly rough sea surface,” *Waves in Random and Complex Media*, vol. 18, no. 4, pp. 641-650, 2008.
- [11] J. Li, L. X. Guo, and H. Zeng, “FDTD investigation on bistatic scattering from a target above two-layered rough surfaces using UPML absorbing condition,” *Progress In Electromagnetics Research*, vol. 88, pp. 197-211, 2008.
- [12] Y. Kuga and P. Phu, “Experimental studies of millimeter wave scattering in discrete random media and from rough surfaces,” *Progress In Electromagnetics Research*, vol. 14, pp. 37-88, 1996.
- [13] S. D. Gedney, “An anisotropic perfectly matched layer-absorbing medium for the truncation of FDTD lattices,” *IEEE Trans. Antennas Propag.*, vol. 44, no. 12, pp.1630-1639, 1996.
- [14] A. Taflove and S. C. Hagness, *Computational Electrodynamics: The Finite-Difference Time-Domain Method*, Artech House, 1995.
- [15] J. S. Juntunen, T. D. Tsiboukis, “Reduction of numerical dispersion in FDTD method through artificial anisotropy,” *IEEE Trans. on Microwave Theory Tech.*, vol. 58, pp. 582-588, 2000.
- [16] A. K. Fung, M. R. Shah, and S. Tjuatja, “Numerical simulation of scattering from three-dimensional randomly rough surfaces,” *IEEE Trans. Geosci. Remote Sensing*, vol. 32, no. 5, pp. 986-995, 1995.
- [17] G. Ruck, D. E. Barrick, W. D. Stuart, and C. K. Krichbaum, *Radar Cross Section Handbook*, vol. 1, Plenum Press, 1970.
- [18] L. Tsang, J. A. Kong and K. H. Ding. *Scattering of Electromagnetic Waves*, John Wiley & Sons. Inc, 2001.
- [19] J. A. Ogilvy, *Theory of wave scattering from random rough surface*, IOP Publishing, 1991.
- [20] J. R. Wang and T. J. Schmutge, “An empirical model for the complex dielectric permittivity of soils as function of water content,” *IEEE Trans. Geosci. Remote Sensing*, vol. GRS-18, pp. 288-295, 1980.